Doxorubicin-Conjugated Immuno-Nanoparticles for Intracellular Anticancer Drug Delivery

By *Meng Shi, Karyn Ho, Armand Keating,* and *Molly S. Shoichet**

A polymeric nanoparticle comprised of surface furan groups is used to bind, by Diels–Alder (DA) coupling chemistry, both targeting anti-human epidermal growth factor receptor 2 (anti-HER2) antibodies and chemotherapeutic doxorubicin (DOX) for targeted, intracellular delivery of DOX. In this new approach for delivery, where both chemotherapeutic and targeting ligand are attached, for the first time, to the surface of the delivery vehicle, the nuclear localization of DOX in HER2-overexpressing breast cancer SKBR-3 cells is demonstrated, as determined by confocal laser scanning microscopy. Flow cytometric analysis shows that the conjugated DOX maintains its biological function and induces similar apoptotic progression in SKBR-3 cells as free DOX. The viable cell counts of SKBR-3 cancer cells following incubation with different nanoparticle formulations demonstrates that the combined DOX and anti-HER2 nanoparticle is more efficacious than the nanoparticle formulation with either DOX or anti-HER2 alone. While free DOX shows similar cytotoxicity against both cancerous SKBR-3 cells and healthy HMEC-1 cells, the combined DOX-anti-HER2 nanoparticle is significantly more cytotoxic against SKBR-3 cells than HMEC-1 cells, suggesting the benefit of nanoparticle-conjugated DOX for cell type-specific targeting. The DOX-conjugated immuno-nanoparticle represents an entirely new method for localized co-delivery of chemotherapeutics and antibodies.

1. Introduction

Polymeric amphiphiles self-assemble upon contact with aqueous environments; the hydrophobic regions of the copolymers spontaneously aggregate driven by hydrophobic association while the hydrophilic segments form the outer corona to maximize their contact with the aqueous environment.[1–9] The interest in polymeric self-assembled nanoparticles as anticancer drug delivery vehicles is growing as a result of their promise in both prolonged circulation time—due to the nanoscale size and hydrophilic outer shell which inhibit phagocytic and renal clearance—and selective tumor accumulation via the enhanced permeability and retention (EPR) effect.[10,11] Having their composition tuned to allow functionalization, polymeric micellar nanoparticles are designed to incorporate targeting ligands by covalent coupling, which combine passive and active targeting in one platform.[2,8,9] An immuno-polymeric nanoparticle system that results from the self-assembly of an amphiphilic copolymer poly(2-methyl-2-carboxytrimethylene carbonate-*co-D,L*-lactide)-*graft*-poly(ethylene glycol)-furan (poly(TMCC-*co*-LA)-*g*-PEG-furan) was recently reported.[2,12] After covalently coupling antibodies to the nanoparticle surface, these immuno-nanoparticles exhibit specific binding with receptor-overexpressing cancer cells. In the current study, the versatility of the function-alized nanoparticle system is extended to couple, for the first time, both antibodies and anticancer agents on the nanoparticle surface (Scheme 1). Through the formation of doxorubicin (DOX) and targeting antibody conjugated immuno-nanoparticles, this novel strategy delivers DOX to the cell nucleus of receptor-overexpressing breast cancer cells in a simple and straightforward manner, while maintaining the pharmaceutical toxicity of DOX.

DOX remains as one of the most effective chemotherapeutic anticancer drugs of the past 50 years and is crucial to the treatment of a range of neoplasms including acute leukemia, malignant lymphoma, and breast cancer.[13] Like all other anticancer agents, however, the high efficacy of DOX is associated with high systemic toxicity to healthy tissue. In particular, the dose-dependent cardiotoxicity induced by DOX is cumulative and life-threatening, making the development of targeted DOX-delivery systems of particular importance.[6,8,12,14–27] Significant progress has been made towards the design and synthesis of polymer-based DOX-delivery systems such as amphiphilic polymeric micelles where DOX is physically encapsulated,[6,8,12,17,20,26] and polymer–DOX therapeutics where DOX is chemically encapsulated by covalent binding to polymers.[23–25,28–30] On the one hand, amphiphilic polymeric micelles have hydrophobic inner cores that load and stabilize DOX via hydrophobic association. Their core–shell nanostructure holds promise for prolonged circulation and eventual accumulation in tumor tissues; however, when physically encapsulated, DOX rapidly diffuses out from the polymeric micelles, likely due to its small size and poor stability in the core.[17,20] On the other

[*] Prof. M. S. Shoichet, M. Shi, K. Ho
University of Toronto, 160 College Street
Toronto, Ontario M5S 3E1 (Canada)
E-mail: molly.shoichet@utoronto.ca
Dr. A. Keating
Cell Therapy Program
Princess Margaret Hospital/Ontario Cancer Institute
University Health Network, Toronto, ON (Canada)
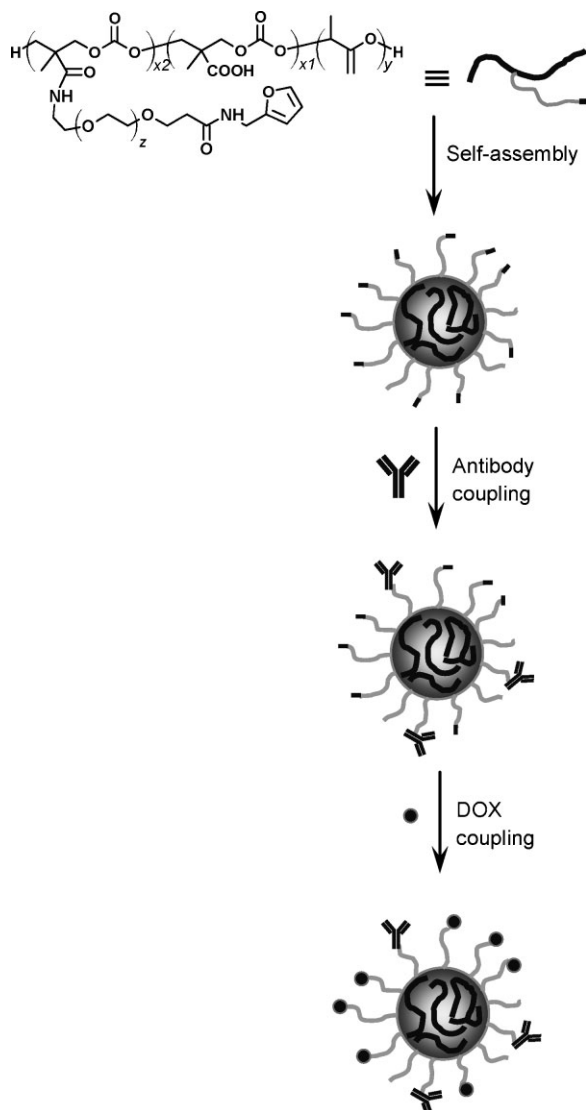
Scheme 1. The preparation of co-labeled antibody- and DOX- polymeric nanoparticles (DOX-conjugated immuno-nanoparticles) using the same Diels–Alder (DA) chemistry for covalent surface modification.

hand, polymer–DOX therapeutics are water soluble polymers that have DOX conjugated via biologically defined linkers that can be cleaved in the lysosomal/endosomal microenvironment, thereby releasing DOX intracellularly. These polymer–DOX therapeutics exhibit good storage stability, low systemic toxicity in circulation, and localized drug release.[28,30] To better control the biocompatibility and selective targeting with precisely structured drug carriers, a new class of polymeric therapeutics, core–shell polymeric nanoparticles, have been designed to have DOX covalently bound to the hydrophobic segments and incorporated into the inner core of the polymeric micelles during self-assembly.[4,5,7,26,31,32] These micellar polymer–drug conjugates combine the advantages of conventional drug-encapsulated polymeric micelles and linear polymer–drug therapeutics. The approach of polymer–drug therapeutics which depends on degradable linkers to target DOX to cell nuclei is limited,

however, by the complex synthesis procedures and the relatively low efficiency of linker cleavage (e.g.<50% over 72 h under stimulus conditions).[4] Regardless of how DOX is specifically encapsulated, it has been incorporated inside these conventional micellar nanoparticles where its nuclear transport is limited.

In this study, we describe the benefit of a polymeric core–shell nanoparticle system where both DOX and antibody targeting ligands are coupled on the nanoparticle surface via a simple conjugation chemistry. The novel DOX-antibody-nanoparticle formulation features the following properties as highly efficient drug delivery vehicles: i) simple preparation obviating the synthesis complexity associated with biodegradable linkers; ii) DOX coupled on the nanoparticle surface favoring its intracellular nuclear transport; iii) antibody targeting ligands achieving specific cellular targeting and intracellular drug delivery via receptor-mediated endocytosis; iv) core–shell nanoscale structure with a hydrophilic corona, promising prolonged circulation time and selective tumor accumulation; v) stable chemical bond between DOX and the polymer suggesting that DOX will be bound to the nanoparticle during circulation, thereby reducing systemic toxicity. We hypothesized that the DOX-conjugated immuno-nanoparticles would both deliver DOX to its target organelle (the cell nucleus) and be specifically cytotoxic to receptor-overexpressing cells.

2. Results and Discussion

2.1. Preparation of DOX-Conjugated Immuno-Nanoparticles

The furan-functionalized amphiphilic copolymer, poly(TMCC-*co*-LA)-*g*-PEG-furan, was synthesized as previously reported,[2] as was its ability to self-assemble into nanoparticle structures via a dialysis procedure.[2,12] As shown in Scheme 1, the hydrophobic segments of the poly(TMCC-*co*-LA) backbone form the dense inner core while the hydrophilic PEG chains orient toward the aqueous solution forming the outer corona upon self-assembly in aqueous environments. The furan functional groups, located at the PEG termini, are easily accessible to maleimide-containing molecules in the aqueous solution. We previously demonstrated that antibodies can be covalently bound on the surface of the polymeric nanoparticles via highly efficient Diels–Alder (DA) chemistry.[2] By calculating the aggregation number of the micellar nanoparticles, it was estimated that antibodies occupied only a few of the PEG-furan groups on the surface, leaving thousands of surface PEG-furan chains available for further modification.[2] In this study, we take advantage of the mild DA reaction conditions to couple DOX-maleimide to those unoccupied PEG-furan chains by the same DA chemistry, resulting in co-labeled DOX-antibody-nanoparticles where both chemotherapeutics and targeting antibodies are on the outside of the nanoparticles (Scheme 1).

Specifically, DOX was modified to introduce maleimide groups at the 13-keto position (Supporting Information Fig. S1), while maintaining the quinone ring intact for drug activity.[13] To construct DOX-conjugated immuno-nanoparticles, self-assembled nanoparticles were surface modified using furan-maleimide DA chemistry with first anti-human epidermal growth factor receptor 2 (anti-HER2) antibodies (aka Herceptin or Trastuzumab) and
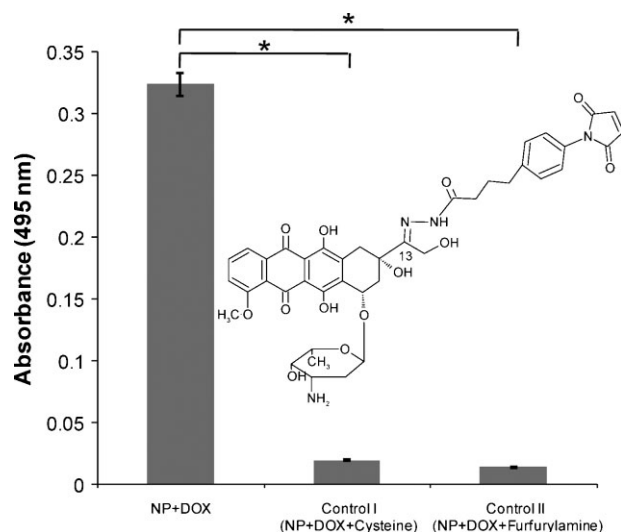
Figure 1. DOX–maleimide coupled to nanoparticles by DA chemistry demonstrates a high UV absorbance associated with DOX coupling whereas the controls have minimal UV absorbance. In Control I, the maleimide on DOX was quenched with cysteine prior to reaction with the nanoparticles, thereby demonstrating the DA chemistry between DOX–maleimide and nanoparticle–furan. In Control II, the maleimide on DOX was quenched by reaction with furfurylamine prior to reaction with the nanoparticles, further confirming the DA chemistry. The inset picture shows the chemical structure of maleimide-modified DOX. Data are the mean $\pm$ SD of three separate experiments. * indicates significantly different by a t-test $p < 0.01$.

then DOX (Scheme 1). DOX-maleimide was coupled to the immuno-nanoparticles in MES buffer (pH 5.5) at room temperature, overnight. As shown in Figure 1, nanoparticles incubated with maleimide-modified DOX showed high UV absorbance at 495 nm (from DOX) indicating that the maleimide-modified DOX was coupled to the nanoparticles. There was little to no evidence of UV absorbance on the nanoparticles in controls I and II, where the maleimide groups were quenched with either cysteine or furfurylamine, respectively, prior to reaction with the nanoparticles, demonstrating that DOX was covalently bound, and not physically adsorbed, to the nanoparticles. DOX-maleimide reacted with 83% of the available PEG-furan groups, resulting in DOX-conjugated immuno-nanoparticles incorporating $20 \pm 3\,\mu g$ DOX per mg nanoparticle (or 2 wt%), a drug loading comparable to that achieved in other polymer-based systems delivering DOX by either physical encapsulation[8] or chemical attachment.[25] While higher drug loadings have been attained with liposomes, the polymeric nanoparticles are being pursued in clinical trials,[33,34] demonstrating the potential of this new innovation for clinical benefit. The hydrodynamic diameter of the DOX-conjugated immuno-nanoparticles was determined by dynamic light scattering to be 125.5 nm with a polydispersity of 0.207, which is a suitable size for selective tumor accumulation in vivo.[10,11]

To test the stability of the chemical bond under physiological conditions, DOX-conjugated immuno-nanoparticles were incubated at 37 °C with one of: a pH 7.4 buffer—the extracellular pH of normal tissue; a pH 5.0 buffer—an acidic environment of extracellular tumor tissue[35] and the interior of lysosomes/

endosomes;[4] and SKBR-3 cells in serum-containing cell media—a HER2-overexpressing breast cancer cell line. During a 72 h period, free DOX was detected in neither the buffer solutions nor the cell culture medium, indicating that DOX is stably bound to the polymers under physiological conditions and when contacting/interacting with cells.

2.2. Intracellular Localization of DOX-Conjugated Immuno-Nanoparticles

By flow cytometry, we previously demonstrated that the anti-HER2 immuno-nanoparticles bind specifically with SKBR-3 cells whereas both IgG1κ isotype control nanoparticles and blank nanoparticles exhibit little binding with SKBR-3 cells, demonstrating minimal nonspecific interaction and physical adsorption.[2] To assess the relative internalization rates of the immuno-nanoparticle formulations and their intracellular localization, confocal laser scanning microscopy (CLSM) was used to visualize the timecourse localization of Alexa 488 fluorescently labeled nanoparticles after incubation with SKBR-3 cells in serum-containing cell media (see Supporting Information Fig. S2 for the fluorescent labeling of blank nanoparticles or immuno-nanoparticles). Blank nanoparticles (NP) presented little surface binding and intracellular internalization at all the time points studied (Fig. 2A). In contrast, anti-HER2 immuno-nanoparticles (NP-aHER2) presented high surface binding at 4 °C (but no internalization because antibody-mediated endocytosis is inhibited at 4 °C) and continuous intracellular accumulation via antibody-mediated endocytosis at 37 °C (Fig. 2B). Since the nanoparticles bind to the SKBR-3 cells specifically via an antibody-mediated interaction and the nanoparticles are comprised of several thousand polymer chains that are modified with either a fluorescent tag or an antibody (or neither, but not both because there is an average of one PEG graft per backbone), it is likely that the fluorescence observed within the cells treated with NP-aHER2 is that of intact immuno-nanoparticles and not free fluorescent-tagged polymer chains. Interestingly, the internalized NP-aHER2 accumulated predominantly in the cell cytoplasm and not the cell nucleus, which is consistent with the intracellular fate of other reported polymeric drug delivery systems: intact drug carriers are internalized via receptor-mediated endocytosis and remain in the cytoplasm[17,27,36–40] likely due to the lack of an active nuclear transport pathway.

DOX-conjugated nanoparticles (irrespective of antibody presence) exhibited different intracellular localization behaviors: when incubated with SKBR-3 cells at 4 °C for 30 min, nanoparticles conjugated with DOX alone (without anti-HER2) exhibited no surface binding to SKBR-3 cells yet modest intracellular DOX accumulation was detected (Fig. 2C), suggesting a route for internalization other than antibody-mediated endocytosis. DOX-conjugated anti-HER2 immuno-nanoparticles (NP-aHER2-DOX) exhibited both surface binding and intracellular DOX accumulation at 4 °C (Fig. 2D). Interestingly, when incubated with SKBR-3 cells at 37 °C, the red fluorescence from DOX was observed in both the cytoplasm and the cell nucleus for both NP-DOX and NP-aHER2-DOX. After 6 h of incubation, the intense DOX fluorescence was localized predominantly in the cell nucleus where much stronger fluorescence intensities were
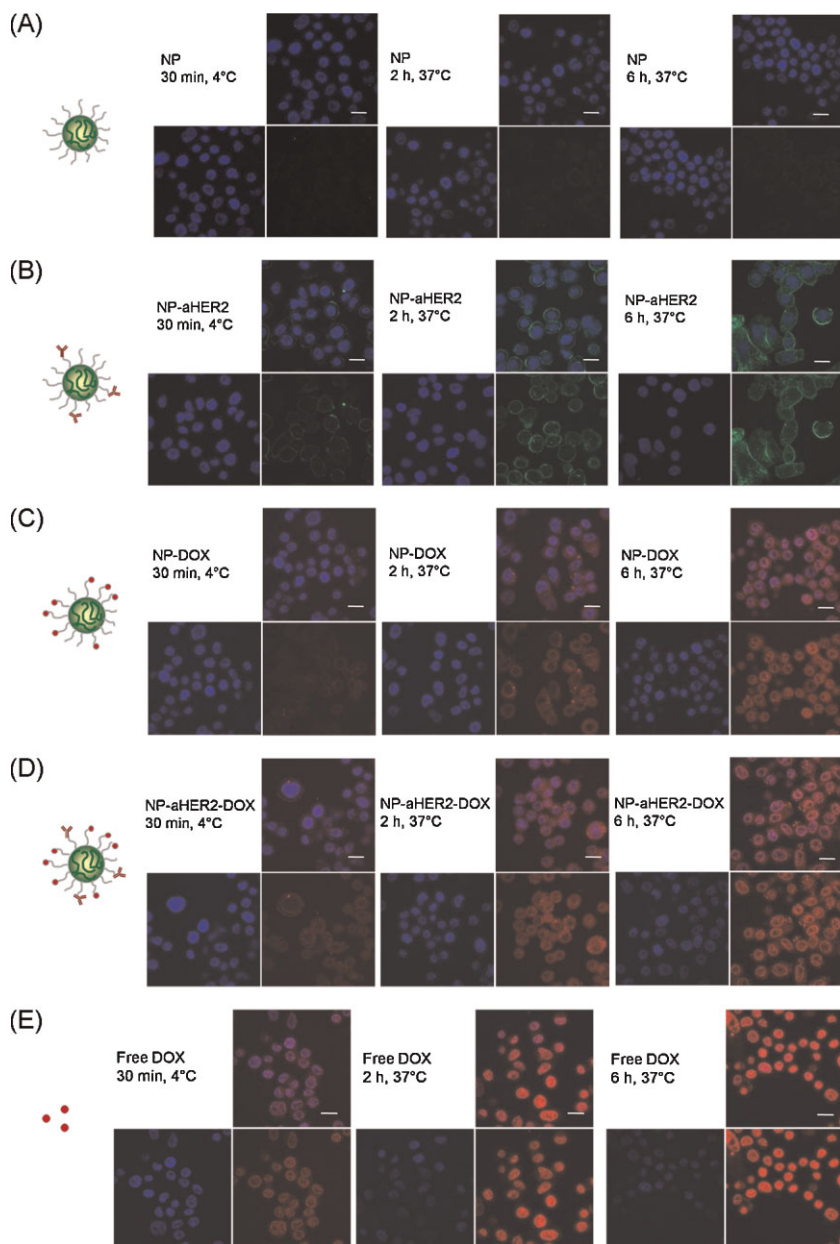
Figure 2. The intracellular localization in SKBR-3 cells, cultured in serum-containing media, was visualized by confocal laser scanning microscopy (CLSM) over time, first at 4 °C and then at 37 °C, for A) blank nanoparticles (NP); B) nanoparticles modified with anti-HER2 (NP-aHER2); C) nanoparticles modified with doxorubicin (NP-DOX); D) nanoparticles modified with both anti-HER2 and doxorubicin (NP-aHER2-DOX); E) free DOX. The blue fluorescence represents DAPI-stained cell nuclei and the red florescence represents DOX. In (A) and (B), where DOX is absent, the nanoparticles were labeled with Alexa 488 (green fluorescence) for visualization. For each condition, the upper right image is a merge of all channels; the lower left is the DAPI blue fluorescence of the cell nucleus; and the lower right is the red or blue fluorescence from DOX or Alexa 488, respectively. Scale bars represent 20 μm.

(Supporting Information Fig. S4). The time-course CLSM images suggest that the intracellular pathway that the DOX-conjugated nanoparticles (both NP-aHER2-DOX and NP-DOX) used to deliver DOX comprised rapid internalization, nanoparticle localization in the cytoplasm and DOX localization in the cell nucleus. Importantly, the nanoparticle-conjugated DOX exhibited the same intracellular fate as free DOX which exclusively stained the cell nucleus (Fig. 2E). Using multiple-labeled DOX-, aHER2- and Alexa 647-polymeric chains that comprise a given nanoparticle (see Supporting Information Fig. S5, the preparation of multiple-labeled nanoparticles), we were able to distinguish the fluorescence between DOX–polymer and Alexa dye–polymer, even though both are associated with the same nanoparticle, to determine whether intact DOX–nanoparticles or free DOX–polymer chains (but not nanoparticles) were localized in the nucleus. After a 6 h incubation of SKBR-3 cells with nanoparticles modified with all of DOX, Alexa 647 and anti-HER2, the fluorescence associated with Alexa 647-polymer was observed in the cell cytoplasm while DOX fluorescence was observed in the cell nucleus, suggesting that it was those polymer chains conjugated with DOX, not intact DOX–nanoparticles, that were selectively transported to the cell nucleus (Supporting Information, Fig. S6).

The mechanism for the nuclear localization of DOX-conjugated polymers is likely similar to that of free DOX because the conjugated DOX nanoparticles have DOX exposed on the surface. Free DOX penetrates through the plasma membrane non-specifically via both electrostatic and hydrophobic interactions with phospholipids[41] and then is likely translocated to the nucleus by the formation of a DOX–proteasome complex.[13,42] This is an active and selective nuclear targeting process which is essential for the drug to reach its target organelle. In the nanoparticle–DOX system, even though DOX is covalently bound to the nanoparticle, it is internalized in the cell nucleus similarly to free DOX (although not as quickly, as shown by the time courses in Fig. 2C–E). The surface-exposed DOX allows the nanoparticles to pass through the cell membrane and accumulate intracellularly even though there is not an active targeting effect (Fig. 2C). Once inside the cells, the polymer-DOX may form a complex with proteasomes similarly as free DOX, which is then selectively transported to the cell nucleus. Notwithstanding the intracellular accumulation of NP-DOX, the intracellular accumulation of nanoparticles modified with both DOX and anti-HER2 was significantly greater due to the additional internalization mechanism of HER2 receptor-

detected for NP-aHER2-DOX than NP-DOX (Fig. 2C and D and Supporting Information Fig. S3, the Z-stacked confocal images). By quantifying the fluorescence intensity of DOX inside the cell body, it was revealed that the intracellular accumulation of NP-aHER2-DOX ($3044 \pm 381 \, \mu m^{-2}$) was significantly higher than that of NP-DOX ($2203 \pm 136 \, \mu m^{-2}$) after 6 h of incubation

mediated endocytosis (Supporting Information Fig. S4), demonstrating the benefit of incorporating antibody targeting ligands in the nanoparticle system.

Thus, for the first time, DOX is conjugated on the surface of the nanoparticle delivery vehicle and demonstrates not only intracellular DOX delivery, but also nuclear DOX delivery. Compared to the conventional DOX delivery techniques where drugs are incorporated inside and DOX nuclear transport is limited, the new formulation of DOX-conjugated immuno-nanoparticles localize DOX to the cell nucleus in a straightforward fashion, suggesting that it is a therapeutically effective drug delivery system for nuclear DOX delivery.

2.3. Induction of Apoptosis Using DOX-Conjugated Immuno-Nanoparticles

To investigate how the nuclear localization of polymer conjugated-DOX impacts its ability to induce apoptosis in vitro, a series of flow cytometry experiments was conducted to evaluate the extent to which samples of drug conjugated nanoparticles or free drug induce apoptosis in SKBR-3 cells. Cells were double stained for viability (negative for propidium iodide (PI)) and apoptosis (positive for Annexin V-FITC). Incubated with SKBR-3 cells in serum-containing media at a concentration of 1.75 μg mL^{-1} DOX-equivalent for 24 h, NP-aHER2-DOX resulted in 9.5% early apoptotic cells (positive for Annexin V-FITC only) and 15.4% late apoptotic cells (double positive for Annexin V-FITC and PI) (Fig. 3A), indicating that polymer-conjugated DOX induced similar apoptotic progression in SKBR-3 cells as free DOX (Fig. 3B) and the biological function of DOX was retained following conjugation to the polymer. As compared to 7.2% of cells in early apoptosis and 8.8% in late apoptosis after treatment by NP-DOX (Fig. 3C), the enhanced apoptosis induced by NP-aHER2-DOX is likely due to the enhanced intracellular uptake associated with antibody mediated endocytosis. Interestingly, anti-HER2 alone and anti-HER2-nanoparticles failed to trigger apoptosis or cell death in SKBR-3 cells (Fig. 3D and E), as the mechanism of action of anti-HER2 with SKBR-3 cells is believed to mainly inhibit cell growth by inducing diminished receptor signaling.[43,44] Importantly, little apoptosis or cell death was observed in controls that had SKBR-3 cells grown in media alone (Fig. 3F).

2.4. Selective Reduction in Cell Viability Using DOX-Conjugated Immuno-Nanoparticles

To gain further insight into the mechanism of NP-aHER2-DOX activity in vitro, the viable cell counts of SKBR-3 cancer cells following incubation with different nanoparticle formulations were compared using a standard tetrazolium MTS assay. Because this assay cannot distinguish between reductions in cell number due to cell death (DOX) versus decreased proliferation (anti-HER2), decreases in the viable cell count normalized to the controls represents reductions from both sources; hereafter, the combined reduction is referred to as the effective cytotoxicity. Figure 4 presents the effective cytotoxicity as a function of DOX-equivalent concentration after incubating SKBR-3 cells with nanoparticle samples or free DOX in serum-containing cell media. NP-aHER2-DOX demonstrated greater effective cytotoxicity than NP-DOX at all the DOX concentrations tested. While neither anti-HER2 nor NP-aHER2 induced apoptotic cell death (Fig. 3D and E), effective cytotoxicity was shown in the viable cell assessment, demonstrating that they both inhibited cell growth (Supporting Information, Fig. S7). Thus the decreased viable cell numbers associated with NP-aHER2-DOX vs. NP-DOX likely reflect a combination of two mechanisms: i) apoptosis associated with increased intracellular DOX delivery and ii) inhibited cell growth associated with anti-HER2. While free DOX showed greater effective cytotoxicity than either NP-aHER2-DOX or NP-DOX, the NP-aHER2-DOX improved the effective cytotoxicity over NP-DOX. This is further validated by the IC$_{50}$ values of: NP-aHER2-DOX (5.0 μg mL^{-1} DOX-equivalent), NP-DOX (10.0 μg mL^{-1} DOX-equivalent), and free DOX (0.6 μg mL^{-1}). NP-aHER2-DOX achieved a two-fold reduction of the IC$_{50}$ value compared with NP-DOX, demonstrating the higher efficacy of a combined DOX and anti-HER2 nanoparticle. NP-aHER2-DOX and NP-DOX are less cytotoxic than free DOX under cell culture conditions, likely due to their slower rate of internalization and longer time needed for nuclear transportation relative to free DOX (which was observed in the timecourse CLSM images in Fig. 2). However, core–shell polymeric nanoparticles have the ability to achieve prolonged circulation time, selective accumulation in the tumour tissue and control of the pharmacokinetics of incorporated drugs, which,
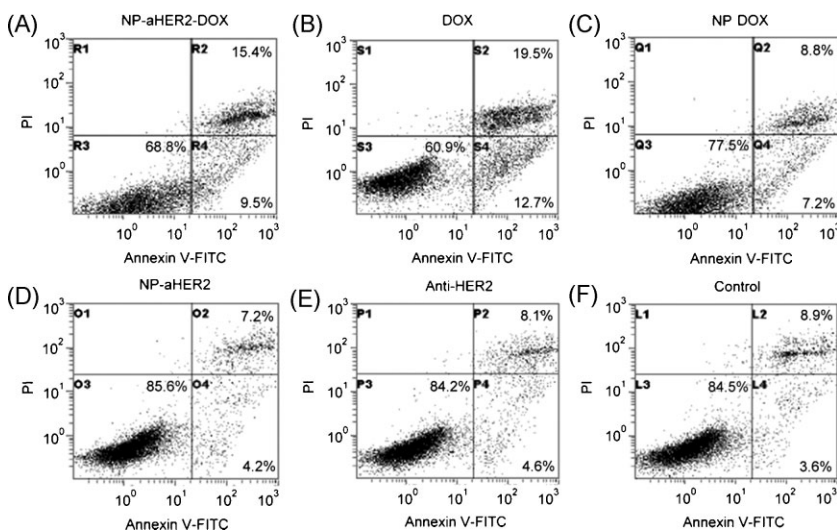
Figure 3. Apoptotic cell populations determined by flow cytometric analysis with Annexin V-FITC and propidium iodide (PI) staining after incubating SKBR-3 cells, cultured in serum-containing media, with A) NP-aHER2-DOX; B) free DOX; C) NP-DOX; D) NP-aHER2; E) free anti-HER2; F) media alone. The bottom-right and top-right quadrants in each panel indicate the populations of early and late apoptotic cells, respectively.
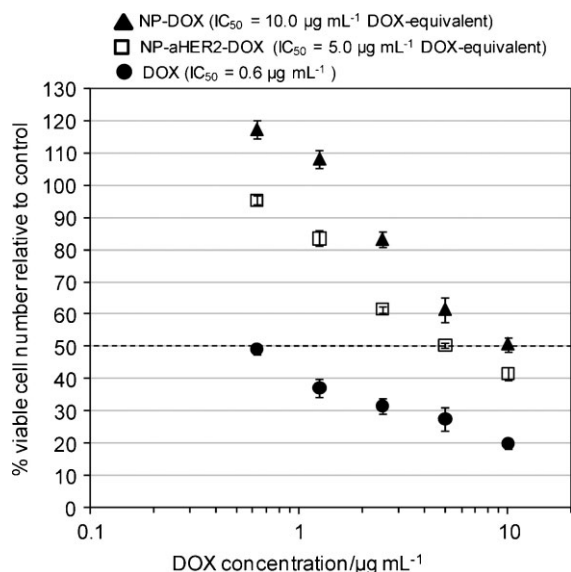
Figure 4. Cytotoxicity of NP-DOX, NP-aHER2-DOX, and free DOX against SKBR-3 cells, cultured in serum-containing media, as a function of DOX-equivalent concentration, as measured by the MTS assay after 72 h of incubation and normalized to control SKBR-3 cells that were cultured in serum-containing media alone. Data are the mean $\pm$ SD of triplicate cultures.

Figure 5. Cytotoxicity results for breast cancer SKBR-3 cells and healthy human microvascular endothelial HMEC-1 cells incubated, in serum containing media, with NP-aHER2-DOX, NP-DOX and free DOX at 5.0 μg mL^{-1} DOX-equivalents (IC$_{50}$ value of NP-aHER2-DOX against SKBR-3 cells after 72 h incubation). Data are the mean $\pm$ SD of three separate experiments; * indicates significantly different by a t-test p < 0.01.

combined with the active targeting mechanism, promises greater specificity to cancer tissue in vivo.

To examine the benefit of nanoparticle-conjugated DOX for cell type-specific targeting, the effective cytotoxicity against SKBR-3 breast cancer cells versus healthy human microvascular endothelial cells (HMEC-1) were compared in the presence of either nanoparticle conjugated DOX or free DOX in serum-containing cell media. It is well known that DOX is highly toxic to both endothelial cells and cardiomyocytes, which accounts for some of the adverse side effects associated with its systemic administration.[45] Since we anticipate intravenous immuno-nanoparticle administration, it is important to limit systemic toxicity by sparing healthy cells, and understand how nanoparticle-DOX and free DOX delivery compare in terms of selectivity for diseased cells. At all time points, free DOX was both similarly cytotoxic to cancerous SKBR-3 cells and healthy HMEC-1 cells and more cytotoxic than either NP-DOX or NP-aHER2-DOX to SKBR-3 cells and HMEC-1 cells. Although DOX-conjugated nanoparticles accumulated in the cytoplasm and cell nucleus of HMEC-1 cells as well (see Supporting Information, Fig. S8), interestingly, the effective cytotoxicity of NP-aHER2-DOX and NP-DOX against HMEC-1 cells was significantly less pronounced than that against SKBR-3 cells (Fig. 5). After 24 h and 48 h incubations at a DOX-equivalent dose of 5.0 μg mL^{-1}, NP-aHER2-DOX resulted in significantly reduced SKBR-3 viable cell number relative to controls (78% versus 63%, respectively) whereas similarly treated HMEC-1 cells were not affected by exposure to NP-DOX or NP-aHER2-DOX, maintaining the same viable cell numbers as the controls. While DOX is more cytotoxic when "free" versus immobilized on the immuno-nanoparticle, the gain in selectivity to cancerous cells is important and significant, promising an enhanced therapeutic efficacy due to both targeted delivery and reduced cytotoxicity to
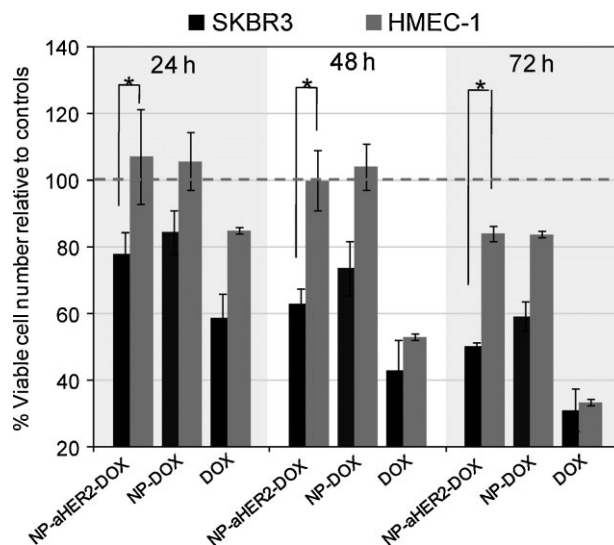
healthy cells. Importantly, in vivo doxorubicin cardiotoxicity is believed to be caused by doxorubicinol, the primary circulating metabolite of doxorubicin formed by the carbonyl reductase at the 13-keto position;[46–48] the lack of a C-13 carbonyl moiety of nanoparticle-conjugated DOX prevents the formation of doxorubicinol, which itself promises reduced cardiotoxicity as compared to free DOX delivery.

3. Conclusions

In summary, a new method for drug delivery has been described: DOX-conjugated immuno-nanoparticles for intracellular drug delivery were developed where both targeting ligands (anti-HER2 antibodies) and chemotherapeutics (DOX) are coupled to a polymeric nanoparticle surface. The nanoparticle-aHER2-DOX formulation delivered DOX intracellularly and localized DOX to the cell nucleus of HER2-overespressing SKBR-3 cells in vitro. The nuclear transport of DOX-polymer was likely mediated by the surface-conjugated DOX. Nanoparticles with both DOX and anti-HER2 exhibited enhanced intracellular uptake and greater apoptosis in SKBR-3 cells relative to nanoparticles with only DOX, and significant specificity to cancerous cells versus healthy cells in terms of cytotoxicity. The results demonstrate the proof of concept for the feasibility of the drug-conjugated immuno-nanoparticles as a new approach to deliver anticancer drugs intracellularly. We expect that the unique structure of the DOX-conjugated immuno-nanoparticles—core-shell nanostructure with both DOX and anti-HER2 chemically conjugated on the nanoparticle surface—may prolong the circulation time, reduce DOX systemic toxicity, and facilitate both passive and

active targeting, thereby making the formulation a therapeutically effective platform for in vivo application.

4. Experimental

Materials: 4-(4-N-Maleimidophenyl)butyric acid hydrazide hydrochloride (MPBH) and N-hydroxysulfosuccinimide (Sulfo-NHS) were obtained from Pierce Biotechnology (Rockford, IL). tert-Butoxycarbonyl protected amine-PEG-activated acid (BocNH-PEG-NHS) was purchased from Nektar Therapeutics (Birmingham, AL). Anti-HER2 (aka Herceptin or Trastuzumab) was obtained from Roche (Mississauga, Ontario, Canada). Alexa Fluor 488 C5-maleimide was purchased from Invitrogen Canada (Burlington, Ontario). Dialysis membranes were from Spectrum Laboratories (Rancho Dominguez, CA). Vectashield mounting medium for fluorescence with DAPI was from Vector Laboratories, Inc (Burlingame, CA). CellTiter 96 AQueous One Solution Cell Proliferation Assay was from Promega Corporation (Madison, WI). Amicon Ultra centrifugal filter devices (MWCO 10k) were from Millipore Corporation (Bedford, MA). All other reagents were purchased from Sigma-Aldrich (Ontario, Canada) and used as received unless otherwise noted.

Cell Culture: The human breast cancer cell line SKBR-3 was used for intracellular localization and cytotoxicity studies. SKBR-3 is a human permanent hypertriploid breast cancer cell line with epithelial features that overexpresses the HER2/c-erb-2 gene product. The cultures were maintained in a HEPA filtered 37 °C humidity controlled incubator, with air supplemented with CO_2 (5%). Cultures were split 1:3 once they reached 70–80% confluence, with medium changes every 2–3 days in between splits. SKBR-3 cells were maintained in T-flasks with vented caps. Their full culture medium was McCoy's 5a medium (Gibco), supplemented with fetal bovine serum (FBS, 10%, HyClone, lot #KPG21605), penicillin (100 U mL^{-1}), and streptomycin (10 µg mL^{-1}). The human microvascular endothelial cell line HMEC-1 was used as a control cell line. HMEC-1 cells are adherent and were selected as a representative healthy cell type that is sensitive to DOX. The cultures were maintained in a HEPA filtered 37 °C humidity controlled incubator, with air supplemented with CO_2 (5%). Cultures were split 1:5 once they reached 70–80% confluence, with medium changes every 2–3 days in between splits. HMEC-1 cells were maintained in T-flasks with vented caps. Their full culture medium is DMEM:Ham's F12 medium (Sigma D6421), supplemented with FBS (10%), L-glutamine (0.5%, Gibco 25030), Hydrocortisone (1ug mL^{-1}, Sigma H0888), epidermal growth factor (EGF, 10 ng mL^{-1}, Sigma E4127), penicillin (100 U mL^{-1}), and streptomycin (10 µg mL^{-1}).

Preparation of DOX-Conjugated Immuno-Nanoparticles: The copolymer, poly(TMCC-co-LA)-g-PEG, was synthesized as previously described [2,12]. The nanoparticles were prepared by dissolving the polymer (40 mg mL^{-1}) in a DMF/borate buffer (50 mM, pH 9.0) (1:1 v/v) and dialyzing against distilled water. The maleimide modified antibody was conjugated with the polymeric nanoparticles by Diels–Alder chemistry [2]. Maleimide-modified DOX was prepared by reacting MPBH with the 13-keto position of DOX. Briefly, DOX (5 mg) and MPBH (15 mg) were dissolved in DMF (0.5 mL). After incubating the solution at 37 °C overnight, MES buffer (500 mM, pH 5.5, 0.5 mL) was added and the solution was passed through a Sephadex G-10 column in MES buffer (500 mM, pH 5.5) for purification. For the coupling of maleimide-modified DOX to the immuno-nanoparticles or the blank nanoparticles, nanoparticle solution (2 mg mL^{-1} in 10 mM PBS buffer of pH 7.4, 1 mL) was added to DOX (0.4 mg mL^{-1} in 500 mM MES buffer of pH 5.5, 85 µg). After incubation at RT overnight, the nanoparticle solution was passed through a Sephadex G-25 column in PBS buffer (10 mM, pH 7.4) to remove unconjugated free DOX. The conjugated DOX was determined using a UV–vis spectrophotometer at 495 nm which is indicative of DOX concentration by comparison to a standard curve. When the feed mass ratio of immuno-nanoparticles to DOX was 2 mg: 85 µg, 47% of the initial feed DOX was coupled to the nanoparticles, resulting in the DOX-conjugated immuno-nanoparticles having 20 ± 3 µg DOX/mg nanoparticle (or 2 wt%).

Intracellular Localization: To observe the nanoparticle localization in cells, cells were incubated with nanoparticle samples under various conditions and fixed for CLSM study. Briefly, SKBR-3 or HMEC-1 cells were seeded on glass coverslips (12 mm circle) in 24-well plates and co-cultured with free DOX or nanoparticle solution (sterile filtered through 0.22 µm filters) under various conditions. After incubation at 4 °C or 37 °C for various time periods, the glass coverslips were taken out and washed twice with fresh PBS to remove any free DOX or nanoparticles. The cells were fixed with paraformaldehyde (4 wt%) and stained with DAPI for nuclear visualization. Accumulation of free DOX or nanoparticle samples in SKBR-3 and HMEC-1 cells was detected using a Zeiss LSM510 confocal microscope. Fluorescence observation was carried out at both 488 nm excitation for DOX/Alexa Fluor 488 detection and 364 nm excitation for DAPI detection.

Apoptosis Assessment by Flow Cytometry: SKBR-3 cells in double-concentrated cell medium were seeded in sterile 6-well plates at a cell density of 5×10^5 cells per well. Equal volumes of DOX or nanoparticle samples in double distilled water (sterile filtered through 0.22 µm filters) were added into each well for treatment with DOX (1.75 µg mL^{-1}). After a 24 h incubation period, non-adherent and adherent cells were collected and washed with cell medium by centrifugation at 1600 rpm for 5 min. After washing using cell medium and then PBS, the cell pellets were resuspended in 1× Annexin V binding buffer (30 µL, Biosource, Camarillo, CA) and Annexin V-FITC (2 µL, BioVision Inc. Mountain View, CA). The cells were incubated on ice for 15 min. After incubation, the cell suspension was transferred to a FACS tube containing propidium iodide (0.6 µg mL^{-1}) and incubated on ice for 4 min. Cell samples were kept on ice until flow cytometry analysis (Cytomics FC500, Beckman Coulter, Mississauga, ON, Canada). The first 10 000 events were acquired by CXP analysis software V2.1.

Cytotoxicity: The cellular cytotoxicity of free DOX and nanoparticle samples against SKBR-3 and HMEC-1 cells was evaluated using a colorimetric MTS assay (3-(4,5-dimethylthiazol-2-yl)-5-(3-carboxymethoxyphenyl)-2-(4-sulfophenyl)-2H-tetrazolium). Cells were seeded in sterile 96-well plates at a seeding density of 1.2×10^4 cells per well in double-concentrated cell medium (100 µL). DOX or nanoparticle samples containing various concentrations of DOX or nanoparticles in double distilled water (100 µL, sterile filtered through 0.22 µm filters) were added for co-culture. Controls had distilled water added instead. At the end of the experiments, MTS (20 µL) was added to each well and the plate was incubated at 37 °C for 2 h. The number of viable cells in each well was determined using a UV–vis spectrophotometer to measure absorbance at 490 nm, indicating cell number by comparison to a standard curve. The % cell number vs. controls is the number of viable cells present after incubating with either DOX or nanoparticle samples relative to those of cells incubated in media alone (controls). The concentrations that resulted in 50% cell viability (i.e., inhibitory concentration 50, IC_{50}) were estimated from the cell viability curve. Three independent experiments were performed.

Acknowledgements

[1] C. Allen, D. Maysinger, A. Eisenberg, *Colloids Surf, B* **1999**, *16*, 3–27.

[2] M. Shi, J. H. Wosnick, K. Ho, A. Keating, M. S. Shoichet, *Angew. Chem.* **2007**, *119*, 6238–6243; *Angew. Chem. Int. Ed.* **2007**, *46*, 6126–6131.

[3] Y. Wang, S. Gao, W. H. Ye, H. S. Yoon, Y. Y. Yang, *Nat. Mater.* **2006**, *5*, 791–796.

FULL PAPER

[4] Y. Bae, S. Fukushima, A. Harada, K. Kataoka, *Angew. Chem.* **2003**, *115*, 4788–4791; *Angew. Chem. Int. Ed.* **2003**, *42*, 4640–4643.

[5] R. Haag, *Angew. Chem.* **2004**, *116*, 280–284; *Angew. Chem. Int. Ed.* **2004**, *43*, 278–282.

[6] C. K. Huang, C. L. Lo, H. H. Chen, G. H. Hsiue, *Adv. Funct. Mater.* **2007**, *17*, 2291–2297.

[7] K. Kataoka, A. Harada, Y. Nagasaki, *Adv. Drug Delivery Rev.* **2001**, *47*, 113–131.

[8] N. Nasongkla, X. Shuai, H. Ai, B. D. Weinberg, J. Pink, D. A. Boothman, J. Gao, *Angew. Chem.* **2004**, *116*, 6483–6487; *Angew. Chem. Int. Ed.* **2004**, *43*, 6323–6327.

[9] V. P. Torchilin, A. N. Lukyanov, Z. Gao, B. Papahadjopoulos-Sternberg, *Proc. Natl. Acad. Sci. U. S. A.* **2003**, *100*, 6039–6044.

[10] D. Peer, J. M. Karp, S. Hong, O. C. Farokhzad, R. Margalit, R. Langer, *Nat. Nanotechnol.* **2007**, *2*, 751–760.

[11] S. M. Moghimi, C. Hunter, J. C. Murray, *Pharmacol. Rev.* **2001**, *53*, 283–318.

[12] M. Shi, M. S. Shoichet, *J. Biomater. Sci, Polym. Ed.* **2008**, *19*, 1143–1157.

[13] G. Minotti, P. Menna, E. Salvatorelli, G. Cairo, L. Gianni, *Pharmacol. Rev.* **2004**, *56*, 185–229.

[14] V. Bagalkot, O. C. Farokhzad, R. Langer, S. Jon, *Angew. Chem.* **2006**, *118*, 8329–8332; *Angew. Chem. Int. Ed.* **2006**, *45*, 8149–8152.

[15] S. Chia, M. Clemons, L. A. Martin, A. Rodgers, K. Gelmon, G. R. Pond, L. Panasci, *J. Clin. Oncol.* **2006**, *24*, 2773–2778.

[16] D. Defeo-Jones, V. M. Garsky, B. K. Wong, D. M. Feng, T. Bolyar, K. Haskell, D. M. Kiefer, K. Leander, E. Mcavoy, P. Lumma, J. Wai, E. T. Senderak, S. L. Motzel, K. Keenan, M. V. Zwieten, J. H. Lin, R. Freidinger, J. Huff, A. Oliff, R. E. Jones, *Nat. Med.* **2000**, *6*, 1248–1252.

[17] E. R. Gillies, J. M. J. Fréchet, *Bioconjugate Chem.* **2005**, *16*, 361–368.

[18] G. L. Griffiths, M. J. Mattes, R. Stein, S. V. Govindan, I. D. Horak, H. J. Hansen, D. M. Goldenberg, *Clin. Cancer Res.* **2003**, *9*, 6567–6571.

[19] C. C. Lee, E. R. Gillies, M. E. Fox, S. G. Guillaudeu, J. M. J. Fréchet, E. E. Dy, F. C. Szoka, *Proc. Natl. Acad. Sci. U. S. A.* **2006**, *103*, 16649–16654.

[20] S. Q. Liu, Y. W. Tong, Y. Y. Yang, *Biomaterials* **2005**, *26*, 5064–5074.

[21] A. N. Lukyanov, T. A. Elbayoumi, A. R. Chakilam, V. P. Torchilin, *J. Controlled Release* **2004**, *100*, 135–144.

[22] J. W. Park, K. Hong, D. B. Kirpotin, G. Colbern, R. Shalaby, J. Baselga, Y. Shao, U. B. Nielsen, J. D. Marks, D. Moore, D. Papahadjopoulos, C. C. Benz, *Clin. Cancer Res.* **2002**, *8*, 1172–1181.

[23] M. Sirova, J. Strohalm, V. Subr, D. Plocova, P. Rossmann, T. Mrkvan, K. Ulbrich, B. Rihova, *Cancer Immunol. Immunother.* **2007**, *56*, 35–47.

[24] K. Ulbrich, T. Etrych, P. Chytil, M. Jelínková, B. Íhová, *J. Drug Targeting* **2004**, *12*, 477–489.

[25] M. J. Vicent, F. Greco, R. I. Nicholson, A. Paul, P. C. Griffiths, R. Duncan, *Angew. Chem.* **2005**, *117*, 4129–4134; *Angew. Chem. Int. Ed.* **2005**, *44*, 4061–4066.

[26] H. S. Yoo, T. G. Park, *J. Controlled Release* **2001**, *70*, 63–70.

[27] H. S. Yoo, T. G. Park, *J. Controlled Release* **2004**, *100*, 247–256.

[28] R. Duncan, *Nat. Rev. Drug Discovery* **2003**, *2*, 347–360.

[29] A. Tang, P. Kopeková, J. Kopeek, *Pharm. Res.* **2003**, *20*, 360–367.

[30] B. Twaites, C. H. Alarcón, C. Alexander, *J. Mater. Chem.* **2005**, *15*, 441–455.

[31] P. A. Bertin, D. Smith, S. T. Nguyen, *Chem. Commun.* **2005**, 3793–3795.

[32] K. T. Oh, H. Yin, E. S. Lee, Y. H. Bae, *J. Mater. Chem.* **2007**, *17*, 3987–4001.

[33] Y. Matsumura, T. Hamaguchi, T. Ura, K. Muro, Y. Yamada, Y. Shimada, K. Shirao, T. Okusaka, H. Ueno, M. Ikeda, N. Watanabe, *Br. J. Cancer* **2004**, *91*, 1775–1781.

[34] Y. Matsumura, *J. Drug Targeting* **2007**, *15*, 507–517.

[35] L. E. Gerweck, K. Seetharaman, *Cancer Res.* **1996**, *56*, 1194–1198.

[36] J. W. Park, K. Hongi, P. Carter, H. Asgari, L. Y. Guo, G. A. Keller, C. Wirth, R. Shalaby, C. Kotts, W. I. Wood, D. Papahadjopoulos, C. C. Bena, *Proc. Natl. Acad. Sci. U. S. A.* **1995**, *92*, 1327–1331.

[37] A. Mahmud, A. Lavasanifar, *Colloids Surf, B* **2005**, *45*, 82–89.

[38] S. H. Kim, J. H. Jeong, K. W. Chun, T. G. Park, *Langmuir* **2005**, *21*, 8852–8857.

[39] R. Shukla, T. P. Thomas, J. L. Peters, A. M. Desai, J. Kukowska-Latallo, A. K. Patri, A. Kotlyar, Jr, J. R. Baker, *Bioconjugate Chem.* **2006**, *17*, 1109–1115.

[40] R. Savić, L. Luo, A. Eisenberg, D. Maysinger, *Science*, **2003**, *300*, 615–620.

[41] G. Speelmans, R. W. H. M. Staffhorst, B. De Kruijff, *Biochemistry* **1997**, *36*, 8657–8662.

[42] K. Kiyomiya, S. Matsuo, M. Kurebe, *Cancer Res.* **2001**, *61*, 2467–2471.

[43] R. Nahta, F. J. Esteva, *Cancer Lett.* **2006**, *232*, 123–138.

[44] S. Lee, W. Yang, K. H. Lan, S. Sellappan, K. Klos, G. Hortobagyi, M. C. Hung, D. Yu, *Cancer Res.* **2002**, *62*, 5703–5710.

[45] S. Wang, E. A. Konorev, S. Kotamraju, J. Joseph, S. Kalivendi, B. Kalyanaraman, *J. Biol. Chem.* **2004**, *279*, 25535–25543.

[46] G. Minotti, S. Recalcati, A. Mordente, G. Liberi, A. M. Calafiore, C. Mancuso, P. Preziosi, G. Cairo, *FASEB J.* **1998**, *12*, 541–552.

[47] H. A. Gambliel, B. E. Burke, B. J. Cusack, G. M. Walsh, Y. L. Zhang, P. S. Mushlin, R. D. Olson, *Biochem. Biophys. Res. Commun.* **2002**, *291*, 433–438.

[48] R. D. Olson, P. S. Mushlin, D. E. Brenner, S. Fleischer, B. J. Cusack, B. K. Chang, R. J. Boucek, Jr, *Proc. Natl. Acad. Sci. U. S. A.* **1988**, *85*, 3585–3589.